Research in Astronomy and Astrophysics, 24:015014 (10pp), 2024 January https://doi.org/10.1088/1674-4527/ad0865

Design and Cryogenic Performance of a Hexapod Platform for a Large Ground-based Wide Field Survey Telescope

Yang Yu[1,2], Xue-Wen Wang[1,2,3], Yu Zhang[1,2,3], Jia-Lin Sun[1,2], Zhen-Bang Xu[1,2,3], and Jian-Li Wang[1,2,3]
[1] Changchun Institute of Optics, Fine Mechanics and Physics, Chinese Academy of Sciences, Changchun 130033, China; yuyang@ciomp.ac.cn, xuzhenbang@ciomp.ac.cn
[2] Chinese Academy of Sciences Key Laboratory of On-orbit Manufacturing and Integration for Space Optics System, Changchun 130033, China
[3] University of Chinese Academy of Sciences, Beijing 100049, China
Received 2023 August 21; revised 2023 October 16; accepted 2023 October 30; published 2023 December 20

Abstract

The thermal gradient is an important factor that causes degradation to the image quality of telescopes. In order to ensure the accurate alignment of the primary focus unit and the primary mirror, the hexapod platform (as a corrector) is investigated in this paper. First, a ground-based telescope with 2.5 m aperture and 3.5 deg field of view is described. The telescope is under construction, and it is expected to be finished in 2023. Second, the hexapod platform with flexure hinges utilized to adjust the primary focus unit is proposed, which is applied as a corrector. Then, the inverse kinematics of the platform is established and an open-loop control system is built based on it. Finally, the cryogenic performance test for the hexapod platform is performed. The experimental results show that the resolution and repeatability of the translation for the hexapod platform can be achieved at the micrometer level. The resolution and repeatability of the rotation can be achieved at the arc-second level. Therefore, the cryogenic performance of the hexapod platform can meet the optical imaging requirements of the wide-field ground-based telescope. The kinematic analysis and cryogenic performance tests in the paper provide a technical reference for the precise alignment of the primary focus unit and the primary mirror, which can improve the imaging quality of the telescope.

Key words: methods: miscellaneous – space vehicles: instruments – telescopes – miscellaneous

1. Introduction

The image quality of an astronomical telescope is affected by the alignment of the secondary mirror and the primary mirror. However, due to the gravity, wind vibration, and temperature, the secondary mirror of an astronomical telescope may be misaligned (Pottebaum & MacMynowski 2006; MacMynowski & Andersen 2010; Angeli et al. 2011; Irarrazaval et al. 2014; MacMartin & Vogiatzis 2014).

Currently, in order to accurately align the secondary mirror within six degrees of freedom (DOF) with respect to the primary mirror, most telescopes use a high-precision adjustment mechanism as an active optical focusing system (Yang et al. 2018; Wang et al. 2023). In addition, the weight of the designed secondary mirror (which can also be referred to as the primary focus unit) can reach 1.2 tons. Therefore, the parallel mechanism with high load capacity is the most suitable choice. The parallel mechanism has been widely used in active optical focusing systems, such as Gran Telescopio Canarias (Casalta et al. 2004), VLT Survey Telescope (Schipani et al. 2007, 2008), and James Webb Space Telescope (Wells et al. 2004; Chonis et al. 2018). It is worth noting that the effect of varying temperatures on optical imaging quality cannot be ignored. Especially for space telescopes, the relevant cryogenic tests are required to be carried out (Streetman & Kingsbury 2003; Wolf et al. 2018). However, for ground-based telescopes with wide fields of view, the effect of cryogenic temperatures on the active optical focusing system has not been investigated and verified in detail. For example, the performance tests for the hexapod platform in Large Synoptic Survey Telescope are conducted only in a room-temperature environment (Neill et al. 2012, 2014; Sneed et al. 2016, 2018). Thus, the relevant research is incomplete. For the hexapod platform being used for active focusing, current research is limited to general testing (Cao et al. 2022). Considering temperature variations will directly affect the imaging quality of the telescope and the performance of electronic components, the cryogenic performance of this platform is required to be verified.

The main contribution of this paper is to present a high-precision hexapod platform with flexure hinges for the primary focus unit, the cryogenic performance of which is excellent enough. First, the assembly of the primary focus unit is presented in Section 2. Then, the structural design of the hexapod platform is described in Section 3. In addition, the inverse kinematics of the hexapod platform is established and

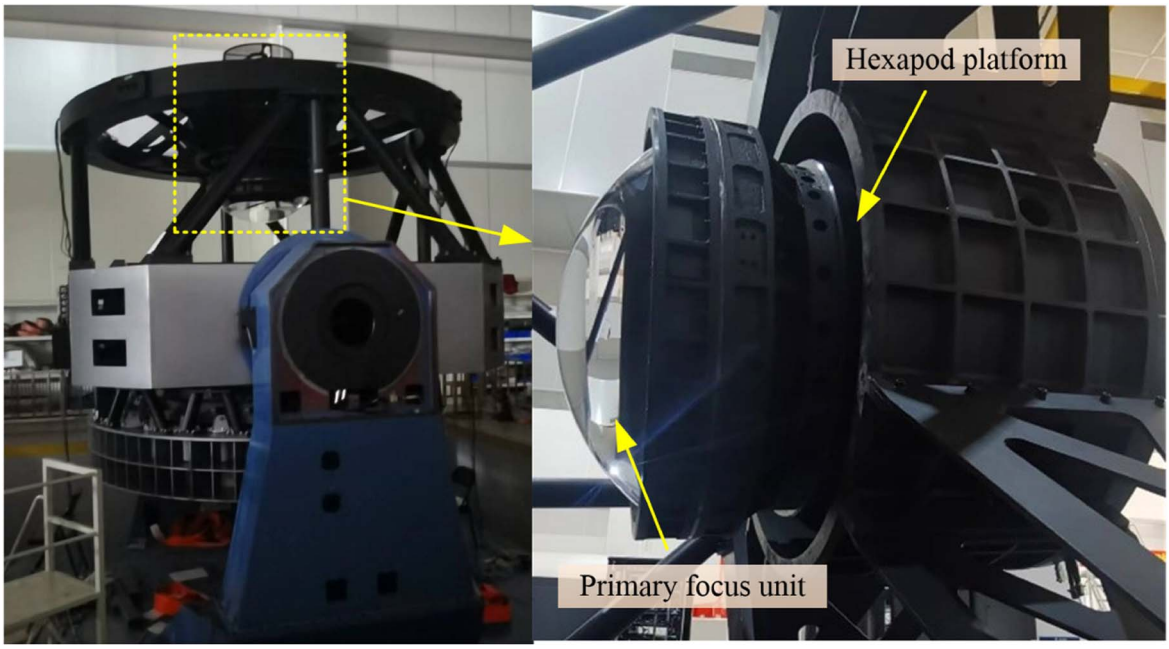

Figure 1. Total integration of the astronomical telescope (left) and primary focus unit (right).

an open-loop control system is built based on it in Section 4. Then, the performance of hexapod platform is tested after the high-low temperature cycling experiments in Section 5. Finally, some conclusions are given in Section 6.

2. Assembly

The integrated assembly of the astronomical telescope is shown in Figure 1. The overall weight of the telescope is about 37 tons, and it consists mainly of a mount structure, a primary mirror, and a primary focus unit. In addition, the envelope of the telescope has a cylindrical shape (when the optical axis of the primary focus unit is vertical), and its height and diameter are approximately 4.5 and 6.5 m. The pose control of the telescope is driven by a brushless torque motor. In order to allow the telescope to be oriented in any direction to cover the area of the sky under investigation, the primary mirror needs to be able to rotate about a vertical axis (azimuth axis) and a horizontal axis (elevation axis).

In addition, the optical configuration of the designed astronomical telescope mainly consists of a Zerodur primary mirror and a primary focus unit, as shown in Figure 2. The Zerodur primary mirror has a 2.5 m aperture and a 3.5 deg field of view. Incident light enters the focal plane of the camera through the primary focus unit, so the primary focus unit can be used as a corrector. It should be noted that the primary focus unit includes six lenses with diameters ranging from 0.29 to 0.87 m.

In the process of actual astronomical observations, the optical alignment of the primary mirror and the primary focus unit can affect the image quality of the telescope. However, the optical alignment is biased by some factors, such as gravity, wind vibration, and temperature. At this time, the actual primary mirror and the primary focus unit deviate from the ideal position and produce optical misalignment, so the optical imaging quality will be reduced. It should be noted that the angular deviation of the primary mirror resulting in the pointing error of the telescope can be easily compensated by controlling the azimuth/elevation angle, which can be achieved by controlling the torque motor. Optical aberration due to optical misalignment between the primary mirror and the primary focus unit can be compensated by controlling the posture of the corrector. Since the primary focus unit needs no less than six degrees of freedom, the hexapod platform is applied as a corrector.

As shown in Figure 3, in order to facilitate disassembly for maintenance, the primary focus unit needs to be assembled as a single unit on the hexapod platform. In addition, the performance of the platform can directly impact the optical alignment of the primary mirror and the primary focus unit. Therefore, in order to maximize the optical imaging quality, the performance of the hexapod platform needs to be explicitly given, as shown in Table 1. The working condition for the hexapod platform is shown in Table 2.

3. Structure Design

As shown in Figure 4, the primary focus unit is fixed to the hexapod platform. The hexapod platform mainly consists of a moving platform, flexure hinges, actuators, and a fixed base. In order to avoid contamination of the optical system, the platform

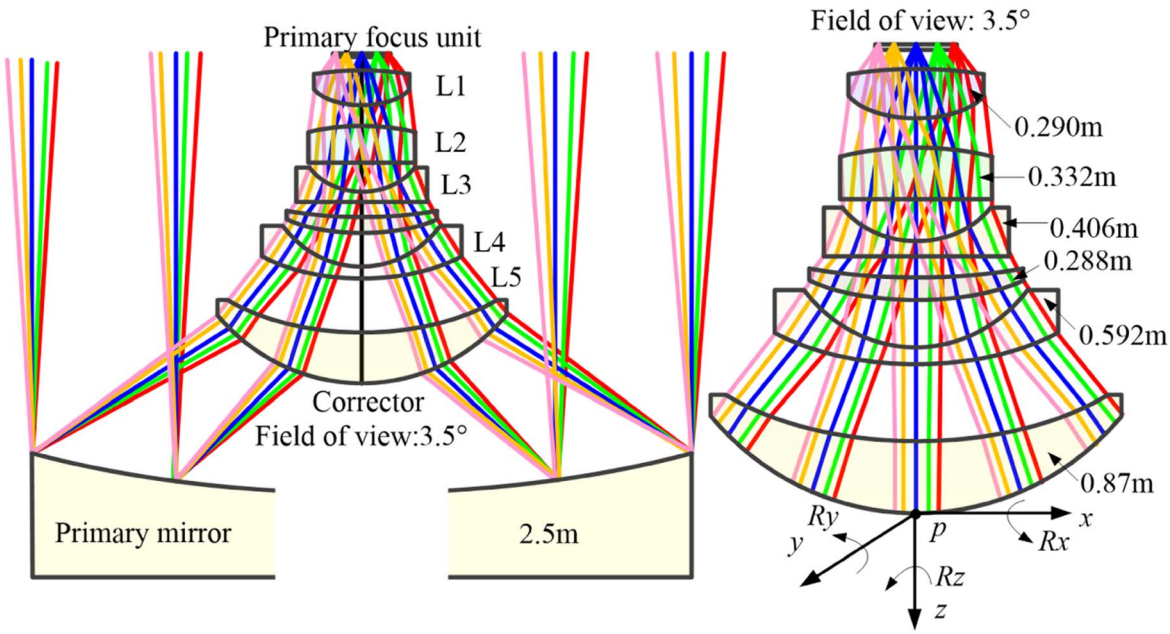

Figure 2. Optical configuration of the astronomical telescope. The primary focus unit consists of a 2.5 m diameter parabolic primary mirror and six lenses (0.29 to 0.87 m diameter).

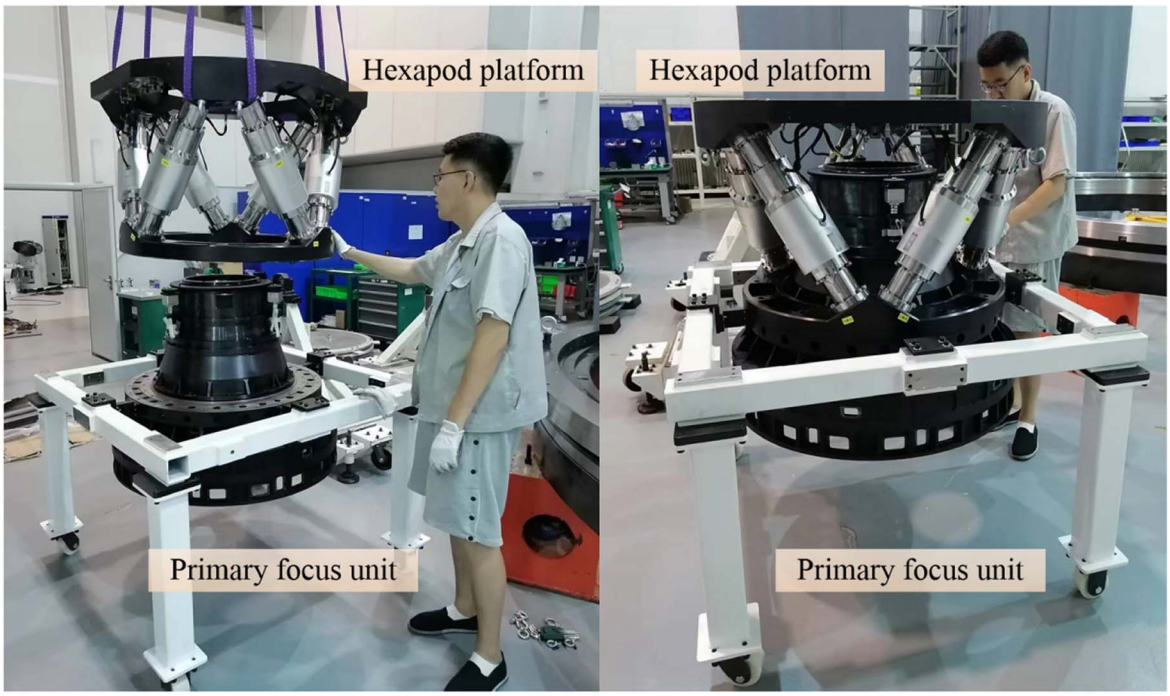

Figure 3. Assembly of the primary focus unit.

needs to be sealed to prevent spillage of lubricant. The hydraulically driven equipment cannot be considered. In addition, the optical system needs to be precise and stable, which means that the precision and stiffness of the platform are very high. Therefore, gas-driven technologies cannot be considered either.

As shown in Figure 5, the actuator mainly consists of a brushless torque motor, an incremental encoder, a planetary roller screw, a hall limit switch, a harmonic gear drive, and an absolute encoder.

Compared to the planetary ball screws, the planetary roller screws have a higher stiffness due to the line contact approach.

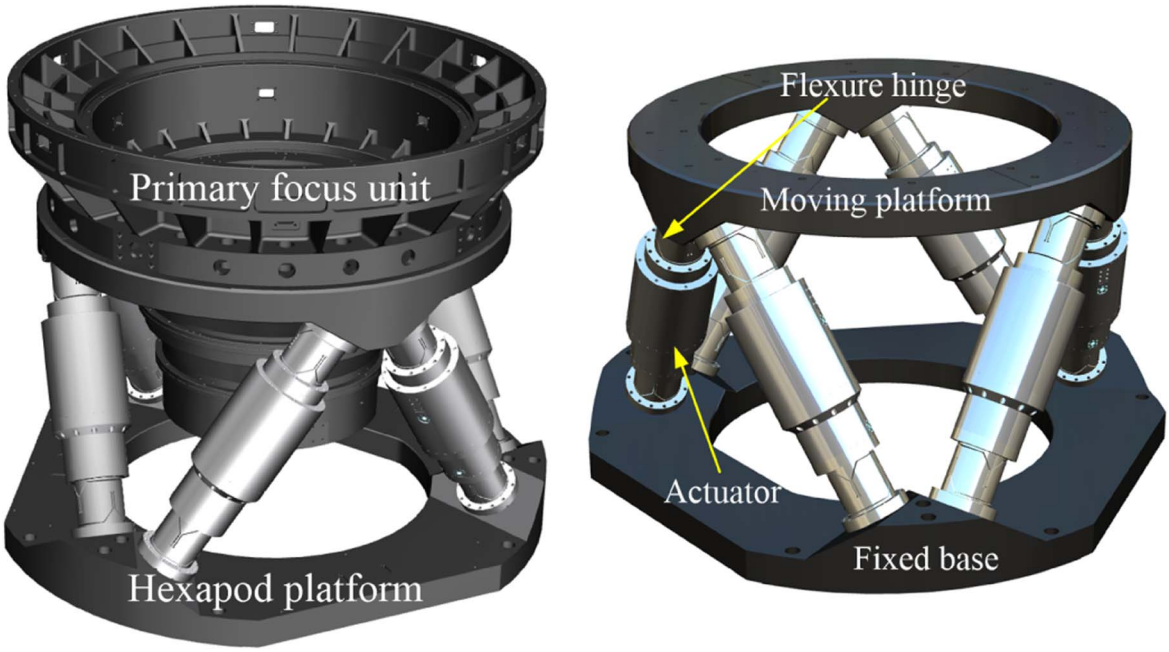

Figure 4. The primary focus unit and the hexapod platform.

Table 1
Performance Indicators of the Hexapod Platform

No	Direction	Stroke	Resolution	Repeatability
1	x	±10 mm	0.5 μm	±3 μm
2	y	±10 mm	0.5 μm	±3 μm
3	z	±15 mm	0.5 μm	±3 μm
4	Rx	±1.5 deg	0.6 arcsec	±1.5 arcsec
5	Ry	±1.5 deg	0.6 arcsec	±1.5 arcsec
6	Rz	±1.0 deg	0.6 arcsec	±1.5 arcsec

Table 2
Working Conditions of the Hexapod Platform

No	Item	Requirement
1	Load weight	1200 kg
2	Power outage	Braking protection
3	Operating temperature	−30°C∼+50°C
4	Storage temperature	−40°C∼+70°C
5	Air pressure	950 mbar∼1050 mbar
6	Working elevation	<2000 m
7	Total mass	<300 kg

In addition, the active optical system operates in an open loop, which requires high bidirectional repeatability. Since the backlash can seriously affect this repeatability, a pre-tightened split-nut arrangement is used to eliminate the backlash.

The hexapod platform has a speed limit in the optical alignment. The output speed of the actuator relies mainly on a harmonic drive (strain wave) gear drive with a gear reduction ratio of 50:1, which can effectively guarantee accuracy, repeatability, and resolution. In addition, compared to conventional gearboxes, the harmonic gear drive has the advantages of small size, light weight, zero backlash, excellent positioning accuracy, and repeatability.

A DC brushless motor has been chosen as the drive element. Compared to DC brushed motors, it offers higher efficiency, better reliability, longer life, and more precise motion control. The fine pitch (1mm lead) of the roller screw and the high gear reduction ratio (50:1) of the harmonic gear drive can limit the torque of the motor, which allows the actuator to be self-locking or non-reversible. Hence, the measure provides the hexapod platform with a power-down holding capability, and it can eliminate the requirement for brakes and the resulting heat.

The absolute encoder is selected as a non-contact high-performance encoder, which can achieve functions such as power-down storage and multi-turn counting. As an encoder mounted at the output, it can accurately record the position of each actuator at any given time. Despite being switched off, the position of the actuator is equally accurate feedback based on the closed-loop control when the power is turned on again. An incremental encoder is mounted on one end of the motor and provides it with speed feedback. Finally, hall limit switches can act as a safety limit.

It is important to note that the rotating joint adopts the flexure hinge rather than the traditional Hook hinge. This hinge has the advantage of no mechanical clearance, no friction, and no assembly required. In addition, the application of the flexure hinge minimizes lag and improves the

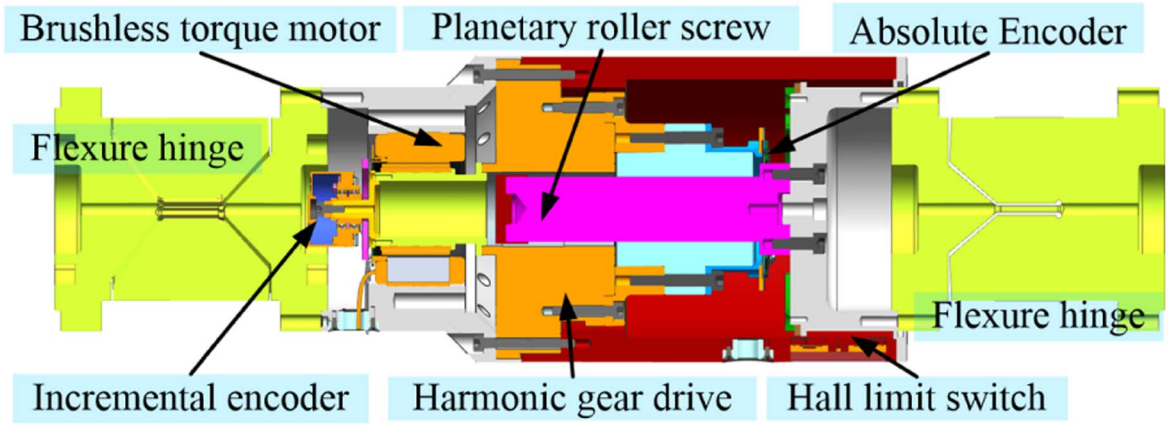

Figure 5. Schematic diagram of the actuator.

overall performance of the telescope. The smoother, lag-free rotation resulting from the flexure hinge facilitates image stabilization. Based on the requirement of a wide field of view, the rotation angle of the designed flexure hinge is required to be not less than 2.5 deg. As the weakest part of the platform, the axial stiffness of the flexure hinge directly affects the pointing accuracy and loading capacity of the platform. In addition, the bending stiffness of the flexure hinge will directly affect the stability of the optical system. Based on the above analysis, the axial and bending stiffnesses of the flexure hinge need to be not less than 3.00×10^{8} N m^{-1} and 1.00×10^{3} N·m rad^{-1}, respectively. The material of the hinge is selected as 17-4 PH. The elastic modulus is 196 Gpa, Poisson's ratio is 0.3, and the yield strength is 1100∼1300Mpa. The axial and bending stiffnesses of the designed flexure hinge are 3.15×10^{8} N m^{-1} and 1.17×10^{3} N·m rad^{-1}, respectively. Most importantly, the von Mises stress of the flexure hinge is an indicator for the evaluation of the fatigue life for a system. The von Mises stress of this hinge is 574 Mpa, which is much less than the yield strength. Therefore, the designed flexure hinge can be applied in the optical systems with wide field of view.

4. Controlling System

4.1. Inverse Kinematic

Currently, the control systems for parallel mechanisms are mainly developed based on the inverse kinematics. For the hexapod platform with flexure hinges, a simplified inverse kinematics model is built to develop the control system. The configuration of the hexapod platform is shown in Figure 6. It is important to note that the center of rotation for the designed flexure hinge can be approximated as being at the geometric center. A_i and B_i are the geometric centers of the upper and lower hinges, respectively. θ_A and θ_B are the distribution angles of the upper and lower hinges, respectively. h is the height of the upper and lower platforms in the configuration. R_A and R_B are the distribution radius of the upper and lower hinges, respectively. In addition, the coordinate systems *P-XYZ* and *O-XYZ* are fixed in the distribution planes of the upper and lower hinges, respectively. Finally, the relevant configuration parameters are required to be specified, as shown in Table 3.

Based on the closed-loop vector relationship, the vectors $\boldsymbol{l}_i$ (i = 1,2,3...6) for each limb can be expressed as

$$\boldsymbol{l}_i = \boldsymbol{OP}_i + \boldsymbol{R}(\alpha, \beta, \gamma) \cdot \boldsymbol{PA}_i - \boldsymbol{OB}_i, \tag{1}$$

where the rotation matrix $\boldsymbol{R}$ (α, β, γ) can be expressed as

$$\boldsymbol{R}(\alpha, \beta, \gamma) = \begin{bmatrix} c\gamma c\beta & c\gamma s\alpha s\beta - s\gamma c\alpha & c\alpha s\beta c\gamma + s\alpha s\gamma \\ s\gamma c\beta & s\alpha s\beta s\gamma + c\alpha c\gamma & s\gamma s\beta c\alpha - c\gamma s\alpha \\ -s\beta & c\beta s\alpha & c\beta c\alpha \end{bmatrix}, \tag{2}$$

where the angle of rotation of the coordinate system *P-XYZ* relative to the coordinate system *O-XYZ* around the x, y and z axes are α, β and γ, respectively. Also, s and c are abbreviated forms of *sin* and *cos*, respectively.

At this point, the length l_i of each limb can be expressed as

$$l_i = \sqrt{\boldsymbol{l}_i \cdot \boldsymbol{l}_i}. \tag{3}$$

In general, the length of each limb does not only depend on its own control inputs, but it is also influenced by other limbs. Therefore, the desired length variation ΔL_{ai} of each limb is referred to as active drive. The length variation ΔL_{pi} due to the influence of other limbs is referred as passive drive. At this point, the length variation ΔL_i of each limb can be expressed as

$$\Delta L_i = \Delta L_{ai} + \Delta L_{pi}. \tag{4}$$

In addition, the angle of rotation of the screw with respect to the nut is $\Delta\theta_i$. The counterclockwise rotation is defined as the positive direction. Therefore, ΔL_i can be expressed as

$$\Delta L_i = (-1)^n \frac{\Delta\theta_i}{2\pi} S, \tag{5}$$

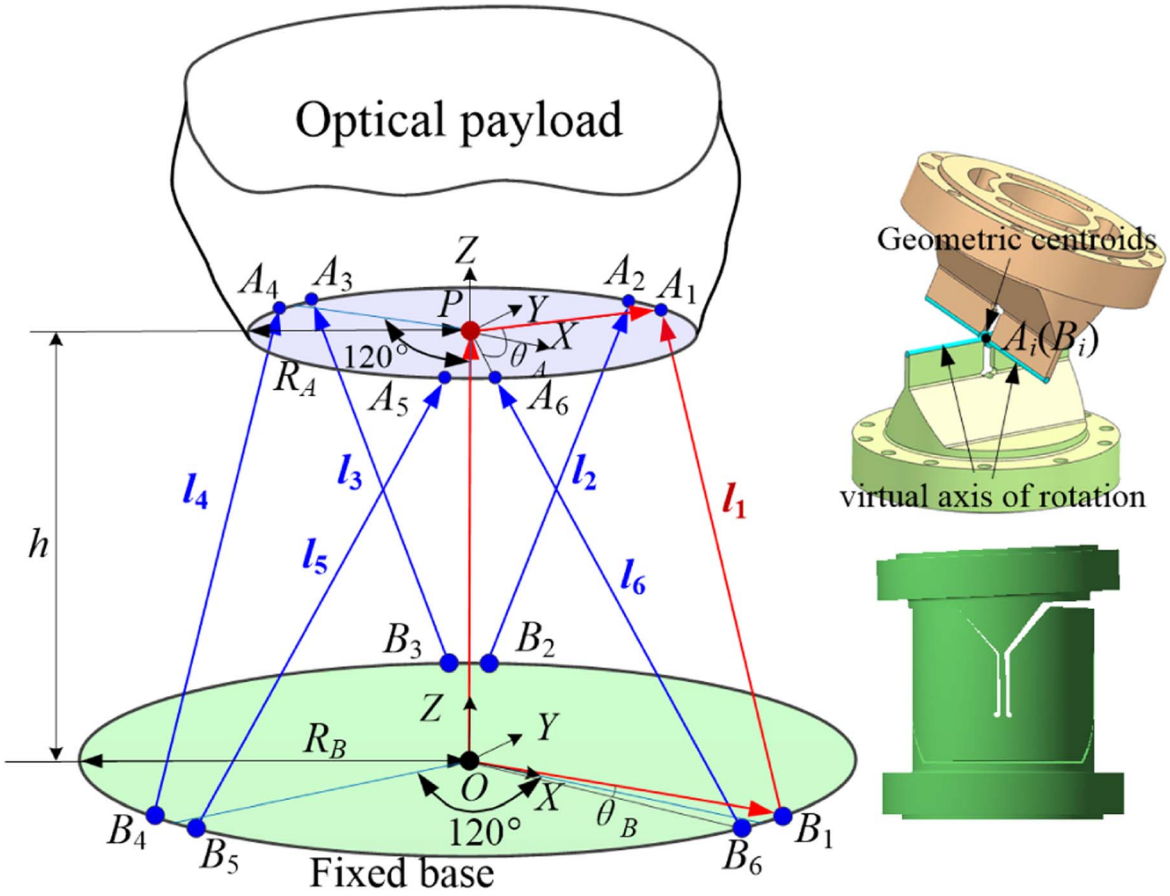

Figure 6. Configuration of the hexapod platform.

Table 3
Working Conditions of the Hexapod Platform

Item	Value
Distribution radius of upper hinges: R_A	379.3701 mm
Distribution radius of lower hinges: R_B	426.9118 mm
Distribution angle of upper hinges: θ_A	92.0309 deg
Distribution angle of lower hinges: θ_B	26.5464 deg
Height of the hexapod platform: h	359.6584 mm

where $n = 1$ if the roller screw is left-handed. Otherwise, $n = 2$. S is the lead of the screw. Then, this inverse kinematics has been verified by the rigid-flexible coupling simulation system (Wang et al. 2023).

4.2. The Principle of the Control System

As shown in Figure 7, an open-loop control system is built based on the established inverse kinematics. First, based on the requirement of the optical alignment, the length variation of each limb is calculated using the desired pose of the platform. Next, the length of each limb is output by the motion controller. Then, a laser displacement sensor is utilized to measure the performance of the platform. Finally, the measured data are analyzed based on the 3σ principle. In addition, absolute encoders make closed-loop position feedback more accurate, and incremental encoders provide velocity feedback to the motor. Since the position and velocity feedbacks are only for these limbs, the control system of the hexapod platform is an open loop.

5. Experiment

5.1. Cryogenic test

In general, the image quality of the telescope is mainly affected by wind vibration, gravitational deformation, and temperature. Temperature gradients not only affect the image quality, but also the stability of the hexapod platform. Too high or too low a temperature may affect the performance of electronic components and the accuracy of the hexapod platform. Therefore, the temperature cycling experiments are required to be carried out.

It should be noted that the hexapod platform is designed to improve the image quality of the telescope through active optical alignment. In other words, the performance of the hexapod platform under the temperature cycling test will

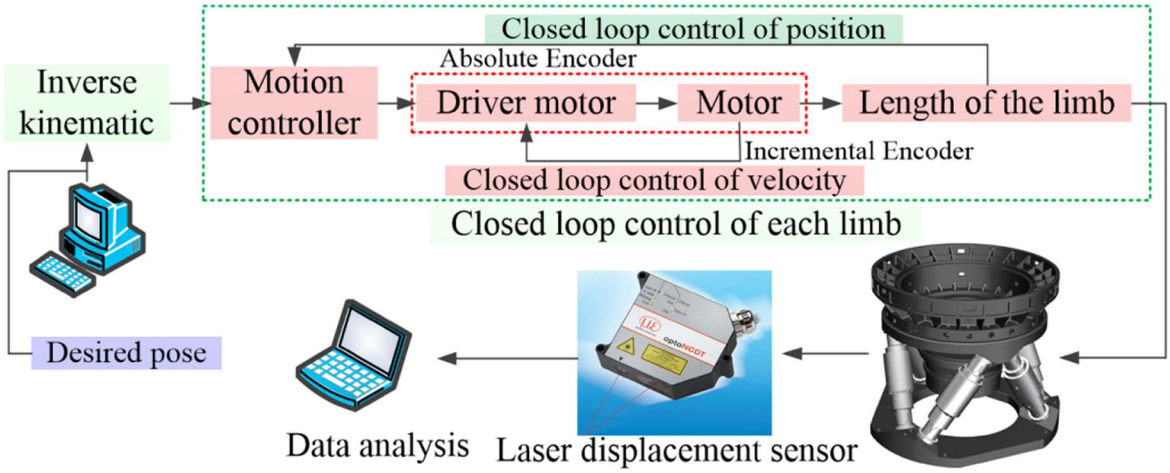

Figure 7. Control system of the hexapod platform.

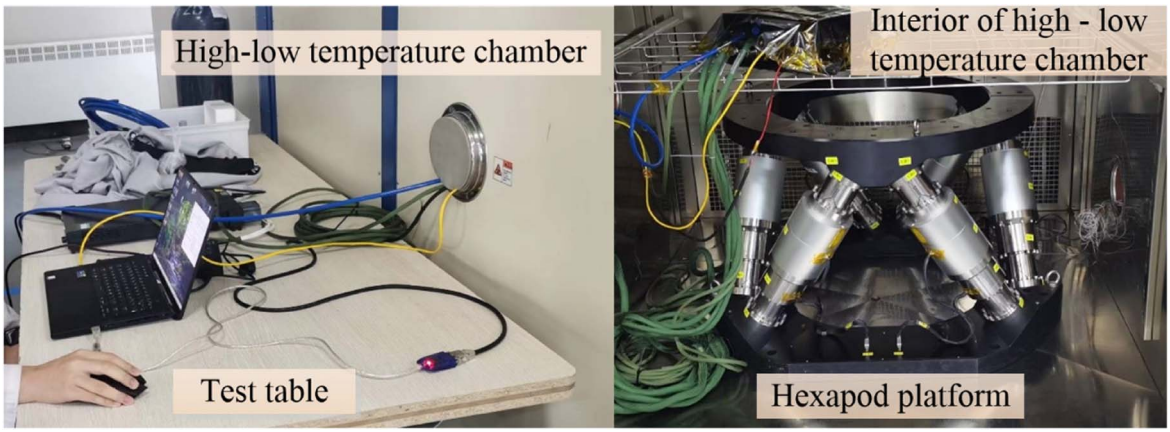

Figure 8. High-low temperature cycling test.

directly reflect the improvement of the actual image quality. It is worth noting that there are drastic temperature variations in the harsh operating environment. Therefore, in order to protect the telescope, the vault needs to be closed after the observation. However, the temperature variations still need to be monitored. The temperature variation of the test is approximately between $+50°C$ and $-30°C$ within a 24 hr period. As shown in Figure 8, the hexapod platform is placed in a high-low temperature chamber. According to Table 2, the operating temperature of the hexapod platform is $-30°C\sim+50°C$ and the storage temperature is $-40°C\sim+70°C$. The temperature difference is relatively large. Based on the requirement, the cyclic variation of temperature is explained in detail, as shown in Figure 9. Temperature reduction is achieved by filling with liquid nitrogen. Temperature increase is achieved by electrical heating. It is important to note that nitrogen is required during the temperature increase to prevent the appearance of atomized water droplets, which are harmful to electronic components. In addition, during each time period of temperature equilibrium, a relevant motion experiment is performed on this platform during the last half hour. Finally, the duration of this experiment is 24 hr, which is designed to mimic the temperature variations throughout the day. It is worth noting that it is difficult to control temperature variations in real time. Therefore, the mimicked temperature variations are only approximately the same as the actual temperature variations. In other words, the maximum and minimum temperatures in the experiment are exactly the same as the actual temperature. In electrical circuits, the current has a significant impact on the performance and safety of the circuit. Therefore, the proper current is essential for the proper operation and extended life of the electrical circuit. The ideal maximum current cannot exceed 21.3 A. The experimental results show that the maximum current does not exceed 11 A, which can meet the requirements. Moreover, the current increases as the temperature decreases. This is because as the temperature decreases, the density of grease in the harmonic reducer and the screw increases, which leads to an increase in damping. Therefore,

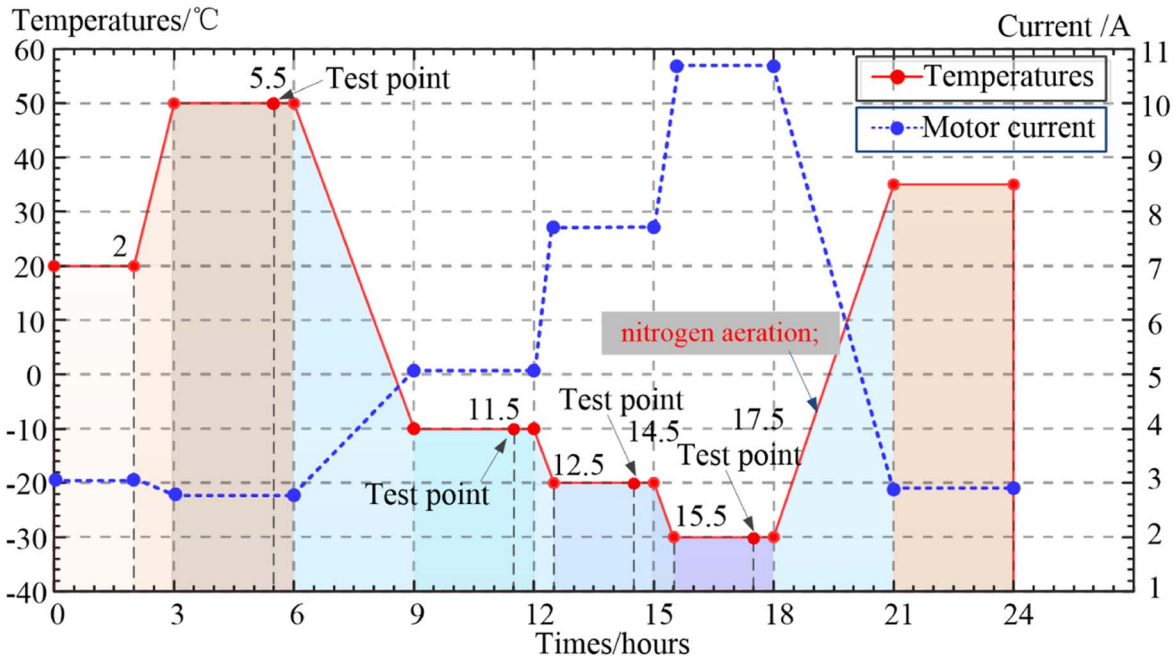

Figure 9. Schematic diagram of temperature control.

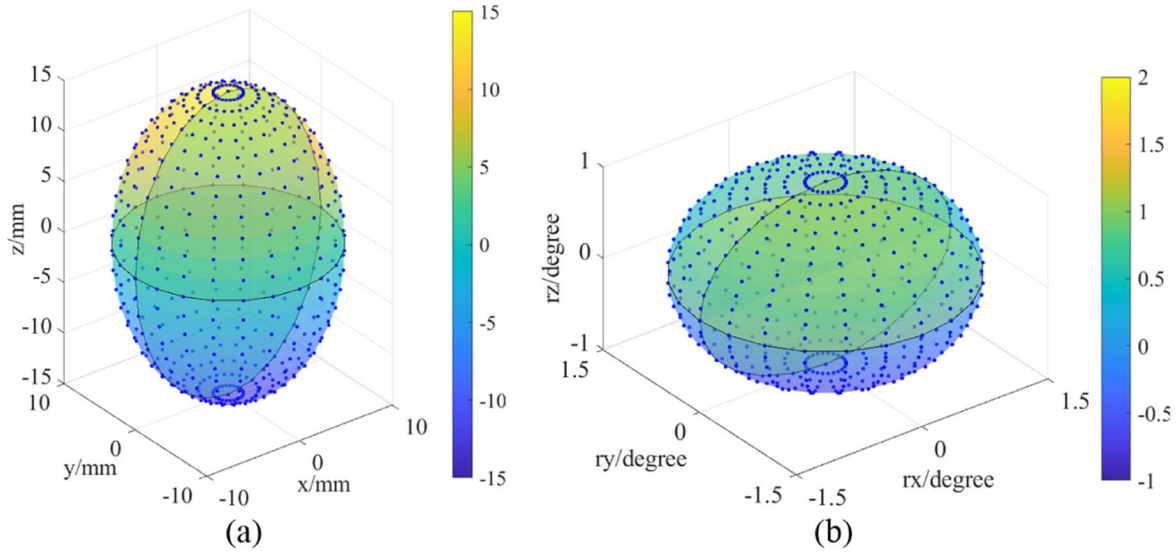

Figure 10. Actual workspace of the hexapod platform.

the motion of the motor needs to overcome the damping of the grease.

5.2. Workspace

In order to verify the effect of temperature variations on the wide field of view, the workspace of the hexapod platform is required to be re-estimated. According to Table 1, the translational strokes along the *x*, *y*, and *z* axes are ±10, ±10, and ±15 mm, and the rotational strokes are ±1.5, ±1.5, and ±1.0 deg, respectively. As shown in Figure 10, the translational and rotational strokes can meet the requirements of the application.

5.3. Resolution

Resolution is an inherent characteristic of the hexapod platform, which refers to the minimum mechanical step. In the assembly of the hexapod platform, despite the application of flexure hinges instead of conventional hinges, mechanical gaps between other components are unavoidable. In addition, other influencing factors include the machining accuracy of the

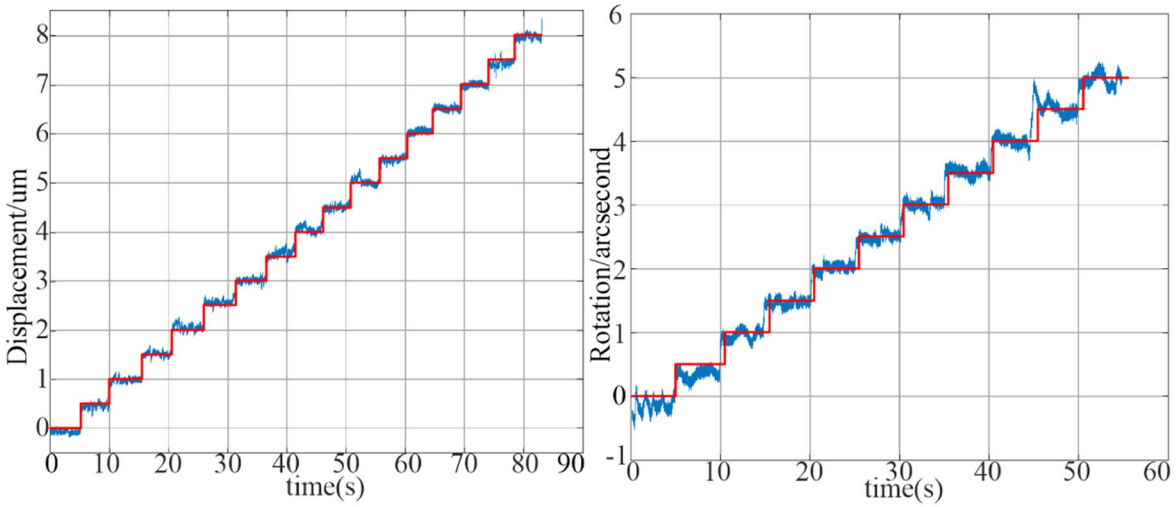

Figure 11. Resolution of translation and rotation.

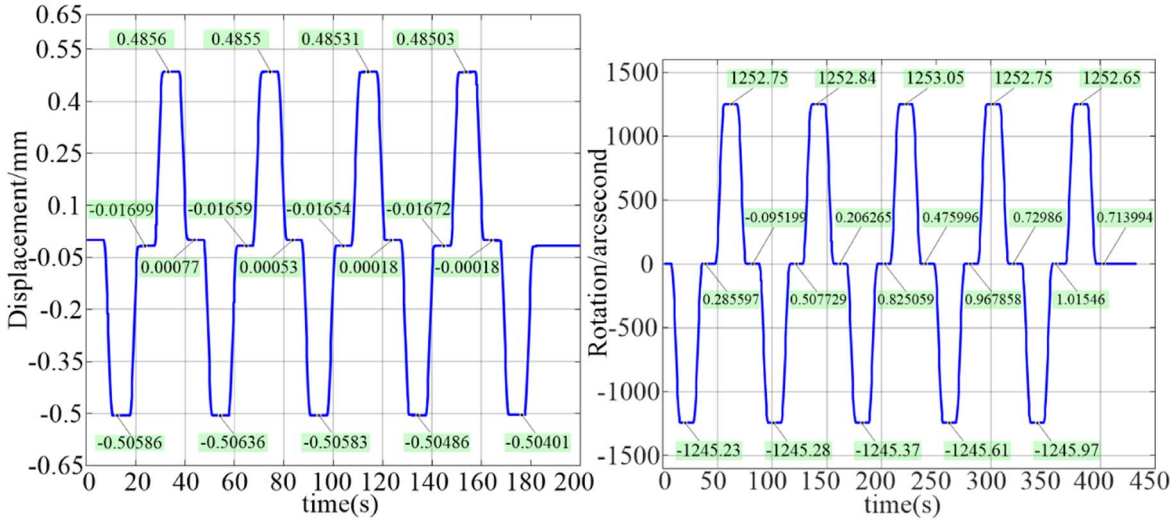

Figure 12. Repeatability of the translation and the rotation for small step sizes.

mounting plane, the resolution of the motor and the screw, the resolution of the encoder, and the torque deformation of the screw. Higher resolution is a guarantee of high imaging quality. According to Table 1, the ideal resolutions of translation and rotation are 0.5 μm and 0.6 arcsec, respectively. The test results show that the actual resolutions of translation and rotation are 0.5 μm and 0.5 arcsec, which can meet the requirements for the application, as shown in Figure 11.

5.4. Repeatability

Repeatability is the consistency between real poses that respond to the same pose from the same direction several times over. It is an indicator of the performance stability of the hexapod platform. The hexapod platform with high repeatability can achieve optical alignment using open-loop control. It is better able to use relevant algorithms to improve the accuracy. According to Table 1, the ideal repeatability of translation and rotation are ± 3 μm and ± 1.5 arcsec, respectively. The experimental small step sizes for translation and rotation are 0.5 mm and 1250 arcsec, as shown in Figure 12. The large step sizes are 10 mm and 1.5 deg, as shown in Figure 13. The experimental results show that the actual repeatability of translation and rotation are ± 2.5 μm and ± 1.5 arcsec, which can meet the requirements.

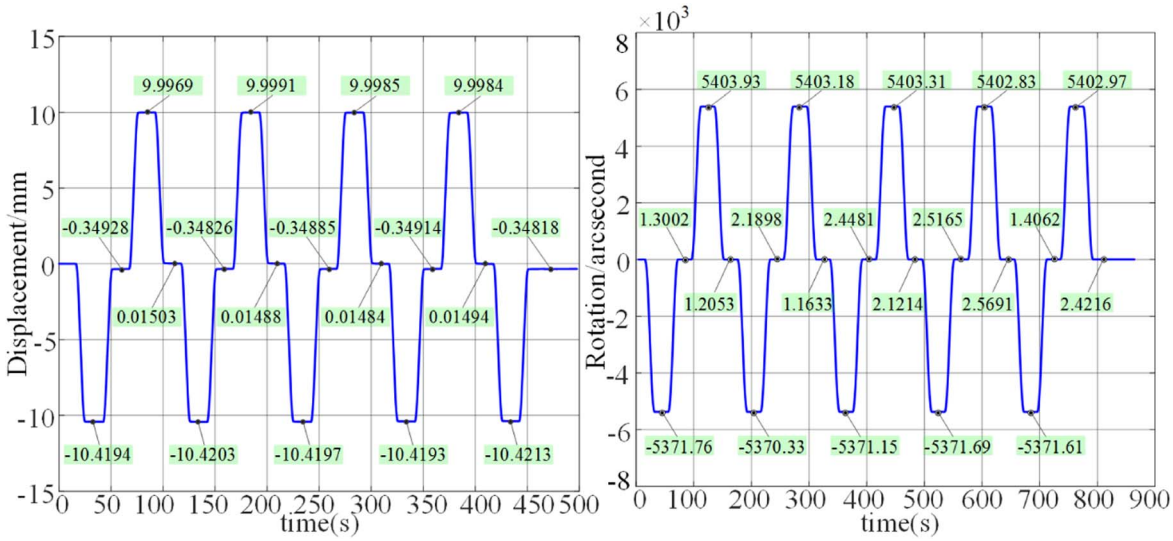

Figure 13. Repeatability of the translation and the rotation for large step sizes.

6. Conclusions

This paper briefly describes the performance evaluation of the hexapod platform for the optical alignment of the astronomical telescope in a high-low temperature cycling environment. First, the detailed structure of the primary focus unit and hexapod platform for the astronomical telescope is presented. Next, a simplified inverse kinematics of the platform is established and an open-loop control system is developed based on it. Then, in order to consider the drastic variation of the ambient temperature, the hexapod platform is subjected to a high-low temperature cycling experiment. The experimental results show that the maximum current does not exceed 11A, which can meet the requirements. Finally, the performance of the hexapod platform is tested. The experimental results show that the workspace can meet the requirements of the wide field of view. The resolution of translation and rotation are 0.5 μm and 0.5 arcsec, respectively. The repeatability of translation and rotation are $\pm$2.5 μm and $\pm$1.5 arcsec, respectively. As a result, the designed hexapod platform maintains excellent performance in the cryogenic experiment, which can meet the requirements of the application.

Acknowledgments

The work was supported by the Jilin Scientific and Technological Development Program (No.20220204116YY) and the National Natural Science Foundation of China (No.62235018 and No.12133009).

References

Angeli, G. Z., Vogiatzis, K., MacMynowski, D., et al. 2011, Proc. SPIE, 8336, 46
Cao, Y., Wang, J., Fan, W., et al. 2022, ApOpt, 61, 3566
Casalta, J. M., Arino, J., Canchado, M., et al. 2004, Proc. SPIE, 5495, 507
Chonis, T. S., Gallagher, B. B., Knight, J. S., et al. 2018, Proc. SPIE, 10698, 1129
Irarrazaval, B., Buleri, C., & Johns, M. 2014, Proc. SPIE, 9150, 725
MacMartin, D. G., & Vogiatzis, K. 2014, Proc. SPIE, 9150, 259
MacMynowski, D. G., & Andersen, T. 2010, ApOpt, 49, 625
Neill, D. R., Gressler, W. J., Sebag, J., et al. 2012, Proc. SPIE, 8444, 169
Neill, D. R., Sneed, R., Dawson, J., Sebag, J., & Gressler, W. 2014, Proc. SPIE, 9151, 772
Pottebaum, T., & MacMynowski, D. G. 2006, JFS, 22, 3
Schipani, P., Ferragina, L., Marty, L., et al. 2007, Proc. SPIE, 6715, 22
Schipani, P., Perrotta, F., Molfese, C., et al. 2008, Proc. SPIE, 7018, 1380
Sneed, R., Neill, D. R., Caldwell, B., et al. 2018, Proc. SPIE, 10700, 1024
Sneed, R., Neill, D. R., Kidney, S., et al. 2016, Proc. SPIE, 9906, 190
Streetman, S., & Kingsbury, L. 2003, Proc. SPIE, 4850, 274
Wang, X., Yu, Y., Xu, Z., et al. 2023, OExpr, 31, 3908
Wells, C., Whitman, T., Hannon, J., & Jensen, A. 2004, Proc. SPIE, 5487, 859
Wolf, E. M., Gallagher, B. B., Knight, J. S., et al. 2018, Proc. SPIE, 10698, 84
Yang, D.-H., Cheng, Y., Wu, C.-C., Fei, F., & Jin, Z.-Y. 2018, RAA, 18, 115